

On-Line Raman Measurement of the Radiation-Enhanced Reaction of Cellobiose with Hydrogen Peroxide

Hope E. Lackey, Heather A. Colburn,* Mariefel V. Olarte, Teresa Lemmon, Heather M. Felmy, Samuel A. Bryan, and Amanda M. Lines



Cite This: *ACS Omega* 2021, 6, 35457–35466



Read Online

ACCESS |



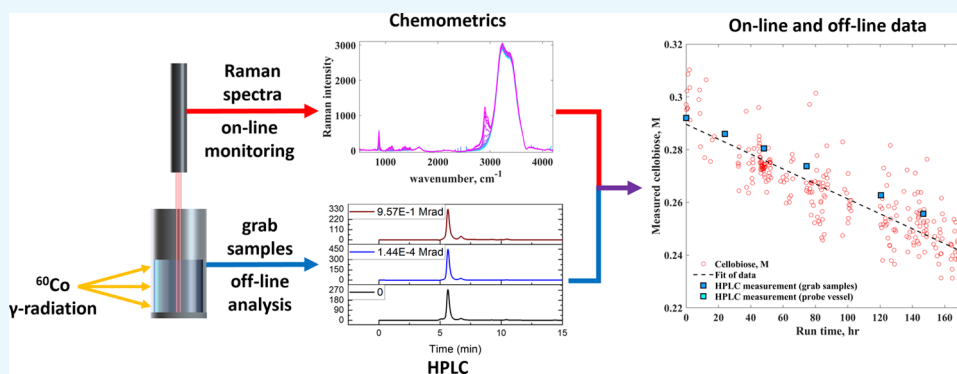
Metrics & More



Article Recommendations



Supporting Information



ABSTRACT: Production of a chemical feedstock as a secondary product from a commercial nuclear reactor can increase the economic viability of the reactor and enable the deployment of nuclear energy as part of the low-carbon energy grid. Currently, commercial nuclear reactors produce underutilized energy in the form of neutrons and gamma photons. This excess energy can be exploited to drive chemical reactions, increasing the fraction of utilized energy in reactors and providing a valuable secondary product from the reactor. Gamma degradation of cellulosic biomass has been studied previously. However, real-time, on-line monitoring of the breakdown of biomass materials under gamma radiation has not been demonstrated. Here, we demonstrate on-line monitoring of the reaction of cellobiose with hydrogen peroxide under gamma radiation using Raman spectroscopy, providing in situ quantification of organic and inorganic system components.

1. INTRODUCTION

Nuclear energy provides a low-carbon alternative to reliably meet energy needs regardless of weather conditions or geological location.^{1,2} It represents a key piece of a diverse energy portfolio that can effectively meet the current goals of lowering the carbon footprint of energy production while maintaining energy security.^{3,4} However, nuclear energy is more expensive than many of the renewable energy generation technologies such as wind and solar, primarily due to the high capital investment required in plant construction, although modern reactors are bridging this gap.^{1,2,5}

As an option to increase the economic viability of next-generation nuclear energy, production of a secondary product, such as a chemical feedstock, would provide an additional product stream and, with that, a secondary source of income.^{1,4,6} A second major barrier to advancing nuclear energy production is public perception, and the ability of unused radiation from nuclear reactors to convert recalcitrant, low-value biomass into desirable products may improve public perception of nuclear reactors.⁷ Combined with net-zero goals in chemical feedstock production, dual-use nuclear systems for

energy and commodity production can have a significant impact on meeting carbon footprint reduction goals.⁵

Currently, nuclear reactors are primarily commodified by using their heat to generate steam for electricity production. There is a large amount of unused energy in the form of photon and neutron radiation that could be exploited to drive chemical processes to produce feedstock materials as a secondary product of a nuclear plant.^{4,8,9} Chemical processing with radiation is not a new concept. In fact, it has been recognized for over half a century that gamma radiation is an excellent source of high-energy photons to drive photochemical reactions.^{8,9} Dow Chemical produced commercial quantities of ethyl bromide using gamma irradiation from a ^{60}Co source in the 1960s and 1970s because it was the most

Received: September 2, 2021

Accepted: December 1, 2021

Published: December 13, 2021



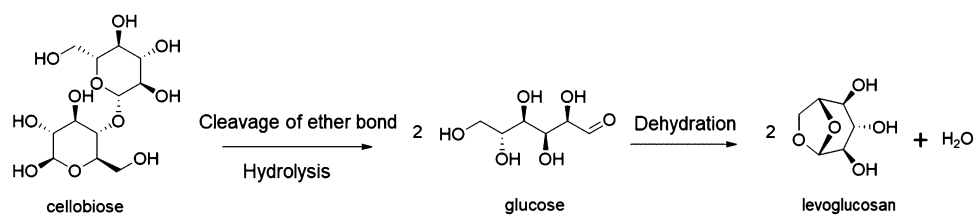


Figure 1. Proposed degradation pathway from cellobiose to levoglucosan.

cost-effective means of production to meet the demand.^{10,11} Numerous other processes have received attention, including the production of ozone and carbon monoxide.^{9,12} However, direct implementation of such processes with nuclear reactors to develop hybrid reactors has not yet seen widespread implementation.

Because of potential economic and environmental advantages, there is a new emphasis on studying feedstock production which can be enhanced by excess gamma, electron, and neutron radiation.^{8,13–19} Lignocellulosic feedstocks have the potential to be a renewable fuel and chemical source,^{13,20–22} and γ -radiation has been investigated for use in the conversion of waste and low-value materials, such as plant straw, into higher-value chemicals.^{23–27} For example, Driscoll et al. discussed the feasibility of including ionizing radiation into a wood-based biorefinery.²⁸ Chung et al. reported the radiation-enhanced degradation of various types of lignocellulosic materials to produce ethanol.²⁹ Unrealized potential exists for utilizing the radiation from nuclear reactors in order to convert lignocellulosic materials into valuable chemicals.

A target system for enhancement via γ -radiation is biomass in solution with an oxidant. Hydrogen peroxide is a common oxidant for use in the chemical conversion of biomass,³⁰ including cellobiose.^{31,32} However, hydrogen peroxide alone does not often meet the desired yield for biomass conversion,³³ so hydrogen peroxide treatment is often used in combination with a catalyst,^{34,35} an acidic or alkaline medium,^{33,36} or the addition of external energy (e.g., heat, pressure).³⁷ The insufficient conversion achieved with unassisted oxidation is discussed further in the [Supporting Information](#), with [Figure S2](#) showing the minimal conversion of cellobiose in hydrogen peroxide when left to react at ambient temperatures. Here, the additional energy imparted to the system comes from γ -radiation.

The focus of this study is the degradation under γ -radiation of cellobiose, a model system for one of the main components of lignocellulosic biomass. Lignocellulose is made up of three main macropolymers: (1) cellulose, a polymer chain of repeating cellobiose (two D-glucose units connected by β -1 \rightarrow 4 linkage) units; (2) hemicellulose, a polymer chain of C₆ or C₅ monosaccharides such as mannose and xylose; and (3) lignin, a polyaromatic constituent material. Of the three main constituents, cellulose is typically the most abundant.³⁸ Anticipated degradation products of oxidized cellobiose are shown in [Figure 1](#). Deng et al. proposed two mechanisms for the formation of glucose from cellobiose in the aqueous phase and in the presence of a supported noble metal catalyst: (1) cleavage of the 1,4'-glycosidic bond between the two monomeric units through hydrolysis to form 2 mol of glucose and (2) cleavage of the glycosidic bond followed by hydrogenation to 1 mol of glucose and 1 mol of dihydroxy-glucose.³¹ In the presence of γ -radiation, a mechanism for

radical-induced cleavage of the glycosidic bond was proposed by Von Sonntag et al.,³⁹ producing glucose isomers and various carbohydrate-derived fragments.

This study extends beyond the scope of previous studies by integrating on-line monitoring of the γ -radiation-enhanced degradation process. Coupling this recently advanced approach to processes that have been explored decades ago can allow researchers to completely reimagine and advance these chemical processes. On-line monitoring provides an in situ and real-time analysis of the chemical process, allowing for more efficient research and development, as well as enabling real-time control and quality assurance of deployed processes. On-line monitoring also contributes to increased safety, particularly in complex and dynamic systems such as hybrid nuclear reactors where both radiological and chemical hazards must be monitored.^{1,40–42}

On-line monitoring of dynamic chemical systems allows for the characterization of complex solution chemistry in real-time.^{43–46} Many approaches to the real-time monitoring of biomass conversion have been successfully deployed using a wide variety of techniques, including but not limited to amperometry,^{47,48} calorimetry,⁴⁹ microbial growth,⁵⁰ and spectroscopy, which is further explored here in the presence of γ -radiation.^{51–56}

Optical spectroscopy provides a uniquely powerful route for on-line monitoring that can identify and quantify a wide range of chemical targets, their speciation, and their oxidation states, often utilizing mature and commercially available technology.⁵⁷ Raman spectroscopy is a good example of this, where probes are physically robust, resisting harsh chemical and radiation conditions.^{58,59} Raman systems also require infrequent calibration, reducing the interruption to experiments or exposure of workers to harsh conditions.⁶⁰ Raman spectroscopy utilizes vibrational approaches that have been demonstrated as useful in previous work, providing valuable insights into reaction parameters such as pH and analyte concentration in both inorganic and organic systems.^{43,46,61–67} Both infrared and Raman spectroscopy have been used successfully in paper and pulp biomass analysis, including on-line monitoring as summarized by Workman.⁶⁸

Here, Raman spectroscopy is used to simultaneously monitor inorganic and organic components of an oxidative reaction system for cellobiose, with hydrogen peroxide as the oxidant. Both hydrogen peroxide and cellobiose are Raman active molecules.^{64,65,68–71} Raman spectroscopy has been used successfully to monitor biomass treatment in real-time,^{51–55} including in a hydrogen peroxide solution.⁵⁴ By developing and utilizing chemometric modeling, on-line monitoring analysis is further advanced. The chemometrics approach can significantly enhance the accurate analysis of optical data and allow for automated conversion of data into quantitative information.^{66,72–74} Chemometric modeling of spectroscopic data has been successfully applied to the analysis of biomass such as

lignin, cellulose, and pulp products, reducing the reliance on slow and costly off-line analyses.^{20,75} Here, partial least squares (PLS) chemometric models are built using Raman spectra for the measurement of two species in a solution, tracking the change in analyte concentration during an ongoing irradiation of cellobiose, a model lignocellulose system. Overall, this provides powerful insights into the radiation-enhanced chemical process and lays the foundation for advancing the use of radiation as an energy commodity.

2. RESULTS AND DISCUSSION

Cellobiose was chosen as the model lignocellulose system. Exposure to hydrogen peroxide simulated an oxidative reaction for the cellobiose. ⁶⁰Co provided γ -radiation so that the chemical changes could be studied in a nonreactor system, providing insights into potential future applications for hybrid nuclear reactors.¹² Two irradiations were conducted on solutions of 0.292 to 0.294 M cellobiose in 1.63 M hydrogen peroxide. Grab samples were collected during the first irradiation and analyzed offline using Raman spectroscopy and high-performance liquid chromatography (HPLC). The second irradiation featured in situ Raman spectroscopy as well as grab sample analysis by HPLC.

2.1. Initial System Characterization Using Grab Samples. An initial run was conducted with 0.292 M cellobiose in 1.63 M hydrogen peroxide inside a stainless-steel vessel, shown in Figure 2A. A ⁶⁰Co source was positioned

spectra were taken for each sample. The dose received by each grab sample is listed in Table 1.

Table 1. Accumulated Dose of Grab Samples of Cellobiose in Hydrogen Peroxide Taken during Two Separate Irradiations

irradiation with off-line monitoring			irradiation with on-line monitoring		
grab sample	duration (h)	cumulative dose (Mrad)	grab sample	duration (h)	cumulative dose (Mrad)
1	0.0	0.00	1	0.0	0.00
2	18.0	1.44×10^{-4}	2	20.9	3.13×10^{-1}
3	62.6	9.57×10^{-1}	3	41.7	6.25×10^{-1}
4	104.2	1.91	4	66.0	9.90×10^{-1}
5	130.0	2.51	5	111.9	1.68
6	155.6	3.10	6	137.9	2.07
7	222.5	4.63	7	164.8	2.47
8	264.7	5.59			

Each grab sample was centrifuged, and the supernatant was transferred to a 10 mm pathlength quartz cuvette, with a Raman probe secured orthogonally to the cuvette face. A schematic of the spectral collection setup is shown in Figure 2C, depicting the location of the sample cuvette to the Raman probe. Spectra were collected with an integration time of 5 s, with 30 spectra collected for each sample. The integration time was selected to acquire an appreciable signal for low-intensity peaks, such as the peroxide peak. The spectra were averaged into a single spectrum in order to reduce noise and reveal low-intensity peaks.

Figure 3A shows the spectral response of the primary peroxide band, while Figure 3B shows the most prominent cellobiose band. The peroxide response peak at 876 cm^{-1} , belonging to the ν_3 O–O stretching, decreases as the dose increases, indicating the consumption of hydrogen peroxide during the reaction.^{69,70} Similarly, the C–H and CH₂ stretching band near 2898 cm^{-1} also decreases, indicating the degradation of cellobiose.^{64,65,76} Overall, this initial scoping study built confidence into chosen chemical constituents and concentration ranges of the training set. It also confirmed that fluorescent degradation products (e.g., hydroxymethyl furfural) were not present in detectable amounts.

In addition to interrogating the grab samples by Raman spectroscopy, the samples were analyzed via HPLC to identify the major degradation products. The chromatograms in Figure 4 show the evolution of peaks with increasing dosage. Four peaks were easily identified, and single component chromatograms are shown in Figure S1. The main peak, eluting at 5.7 min, was assigned to cellobiose, while the peak at 6.7 min was assigned to glucose, the monomer of cellobiose. The peak at 9.6 min was assigned to levoglucosan (1,6-anhydroglucose), while the peak at 10.05 min was identified as formic acid.

The first chromatogram (labeled 0) shows the presence of small peaks aside from cellobiose. This observation may be due to impurities in the starting cellobiose (purity = >98%) or preliminary reactions in the presence of the hydrogen peroxide that occurred during the time between the offline HPLC analysis and the actual sampling. Notwithstanding these considerations, the presence of cellobiose at all dose levels suggests that a substantial portion of the reactant remained unreacted. The presence of dissolved O₂, which was shown to suppress the homolytic cleavage of disaccharides, likely contributed to the incomplete conversion.⁷⁷ However, as

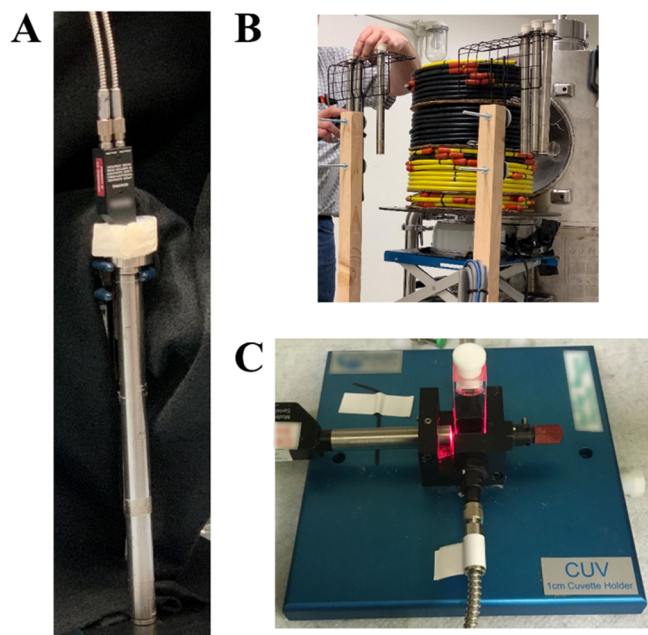


Figure 2. (A) Stainless-steel reaction vessels used during irradiation studies with a 1/4 in. in diameter Raman probe and a foam spacer. (B) Position of the reaction vessels in proximity to the gamma source within the γ -irradiator facility. (C) Cuvette holder used in the collection of grab sample spectra.

in front of the reaction vessels, shown in Figure 2B, creating the irradiation field. The dose rate applied to the samples was 8.0 to 23.0 krad/h over the course of irradiation, with a total dose delivered to the samples of 5.59 Mrads. Grab samples were acquired throughout the exposure during scheduled down-times for the source, for a total of 8 samples, and Raman

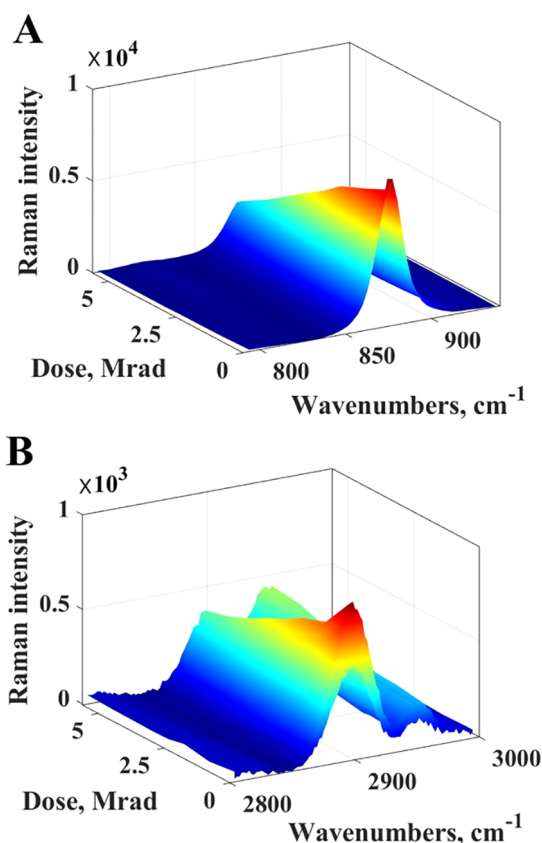


Figure 3. Preprocessed Raman spectra of grab samples from an irradiation of cellobiose in hydrogen peroxide, highlighting the regions for (A) hydrogen peroxide and (B) cellobiose.

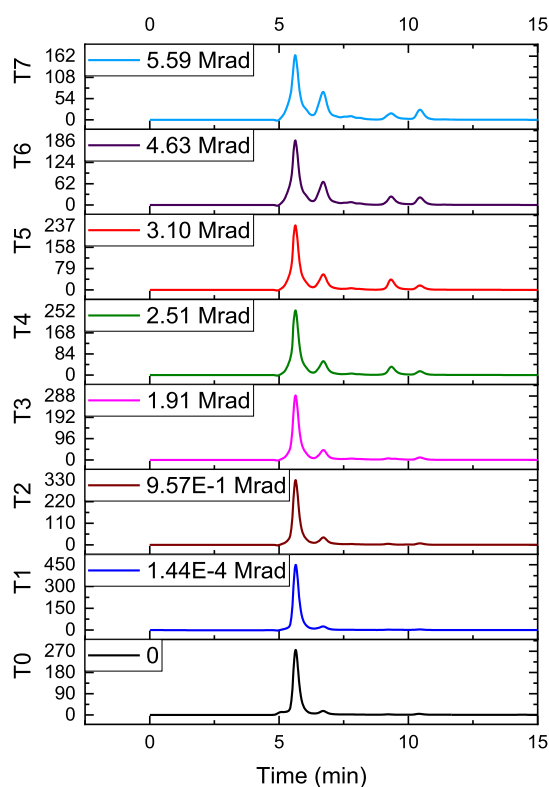


Figure 4. HPLC chromatograms of grab samples at various dose rates.

shown in Figure 5, it is obvious that a higher amount of radiation caused an increased conversion of cellobiose. The

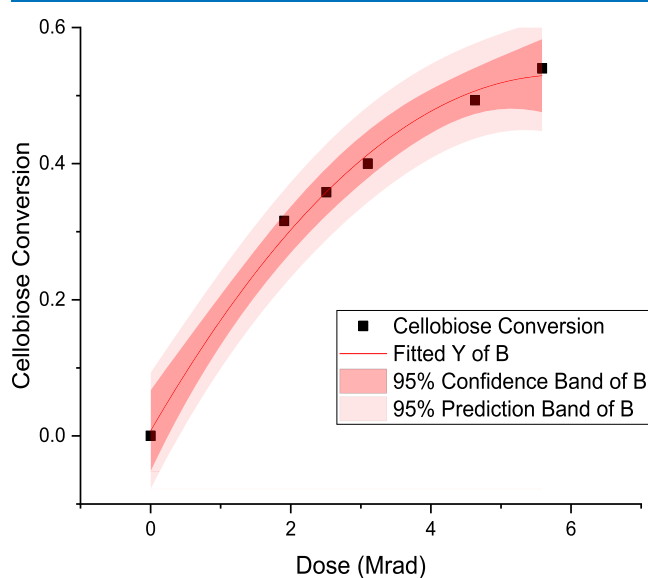


Figure 5. Conversion of cellobiose as a function of dose in grab samples.

second-order curve shows a good fit, with $R^2 = 0.994$. All the calculated cellobiose conversion points were found within the 95% confidence band of the fit. While the temperature was not logged during ongoing irradiations, the low sample concentration and narrow stainless-steel vessel design were expected to allow for the efficient dissipation of heat such that the sample remained at ambient temperature during irradiation.

Glucose is the second most abundant compound present in the samples. It is formed by the hydrolysis of the β -O-4 bonds in cellobiose (Figure 1). The amount of glucose, levoglucosan, and formic acid increased as the dose was increased. It must be noted that levoglucosan and formic acid compounds were not identified in cellobiose radiolysis studies in the absence of hydrogen peroxide.^{39,77}

2.2. Building the Training Set. With Raman and HPLC analyses of grab samples revealing clear changes in the system in response to increasing dose, a training set was created to enable on-line monitoring during an ongoing irradiation via the creation of chemometric models.

While on-line monitoring data was collected in situ during irradiation, training set standards were generated under controlled conditions in the laboratory. Training set samples were designed to capture the spectral fingerprints of products and reactants from the radiation-enhanced degradation, as identified in the grab samples by HPLC and Raman spectroscopy analyses. The training set consisted of samples of hydrogen peroxide ranging from 0 to 1.80 M, cellobiose ranging from 0 to 0.327 M, and combinations thereof. Samples containing the degradation products included 0.0100 to 0.0500 M levoglucosan and 0.0500 to 0.288 M glucose. These concentration ranges were chosen to encompass all expected concentrations of reactants and products of interest that would be encountered during the on-line monitoring. Initially, hydroxymethyl furfural was included as an anticipated product of the cellobiose decomposition with peroxide, but it was not observed in irradiation experiments and was ultimately not included within the final training set. For each sample, 50

spectra were collected at a 10 s integration time with the 1/4 in. Raman probe immersed in the solution in a stainless-steel vessel to match the setup used during irradiations is shown in Figure 2A. The integration time was increased relative to the grab sample set due to the use of a different probe. Additional spectra were collected to produce low-noise, averaged spectra that resulted in improved chemometric model statistics. Figure 6A shows the major bands in Raman spectra of cellobiose

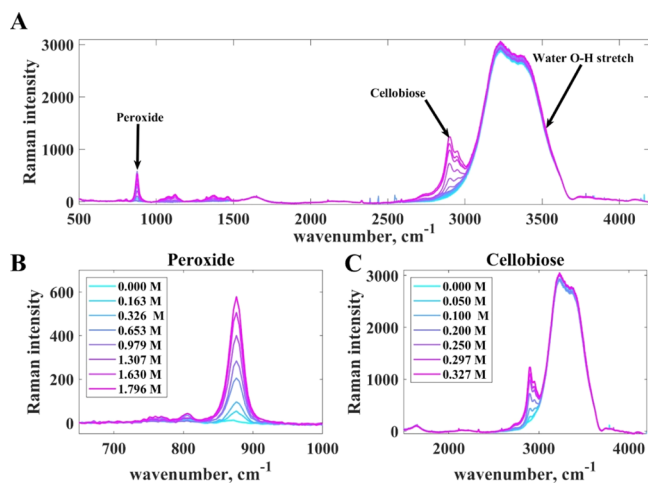


Figure 6. (A) Spectra of mixtures of hydrogen peroxide and cellobiose in deionized (DI) water showing the relative positions of the bands associated with the hydrogen peroxide, cellobiose, and water O–H region; (B) expanded region (650–1000 cm^{-1}) showing spectra of variable hydrogen peroxide concentrations; and (C) expanded region (1500–4200 cm^{-1}) showing spectra of variable cellobiose concentrations.

solutions, including the O–H stretching, which is primarily from water. Figure 6B shows the response of the O–O stretching of hydrogen peroxide, and Figure 6C shows the C–H stretching from cellobiose.

2.3. On-Line Monitoring of the Irradiation-Enhanced Process. A second series of irradiations were completed with a monitoring probe in place, acquiring spectra in real-time during an irradiation. Two samples of ~ 0.293 M cellobiose in 1.63 M hydrogen peroxide were simultaneously irradiated in separate stainless-steel vessels at a rate of 15.0 krad/h for a total dose of 2.47 Mrads. The setup was optimized to enable grab sample verification of the chemical reaction without interrupting continuous on-line monitoring. Grab samples were collected from the first vessel, containing 0.292 M cellobiose, throughout the irradiation, for a total of 7 samples. The 1/4 in. Raman probe was placed in the second vessel containing 0.294 M cellobiose in order to collect spectra in situ throughout the irradiation. The spectra were collected with an integration time of 10 s (to match the training set integration time), and there was a delay of 10 to 30 s in between the spectral collection.

Figure S3 presents the Raman spectra collected over the course of the irradiation, focusing on the hydrogen peroxide and cellobiose fingerprint regions. Cosmic rays and baseline drift, caused by bubble formation on the Raman probe window, can be seen. The effect of these interferences is discussed further below.

2.4. Chemometric Modeling of In Situ Spectral Data. PLS models were built from the training set spectra. Individual

models were built to quantify both peroxide and cellobiose. The spectra included in the training set were preprocessed in order to account for laser power fluctuation and other physical interferences. The preprocessing of the spectral data consisted of the following: a first-derivative using a 15 point cubic Savitzky–Golay smoothing of each spectrum,⁷⁸ normalization of all spectral intensities based on the integrated area under the water band (3030 to 3310 cm^{-1} region), and mean centering of the data. Cross-validation was performed using the venetian blinds method. The Savitsky–Golay filter reduces instrument noise and cosmic ray peaks while also reducing the signal of broad baseline features. The normalization accounts for fluctuation in the laser power and alterations to the light path, as discussed in detail below.

The parity plot of the peroxide model, shown in Figure 7A, demonstrates a linear relationship ($R^2 = 0.999$) between the

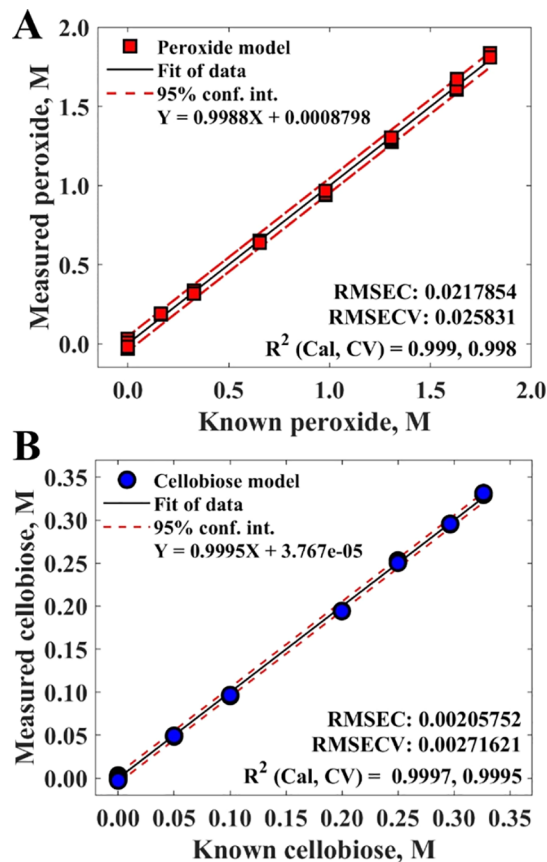


Figure 7. Parity plots for PLS models for (A) hydrogen peroxide and (B) cellobiose; demonstrating a linear relationship ($R^2 = 0.999$ and 0.9997 , respectively) between the known and measured results for each species.

known solution concentration and the concentration of the training set solutions as measured by the model. The root-mean-square error of cross-validation (RMSECV), which can be considered an error on the measurement, is 0.0258, which is very low relative to the starting peroxide concentration of 1.63 M peroxide in the irradiated samples. Similarly, the parity plot of the cellobiose model is shown in Figure 7B, providing a linear fit with $R^2 = 0.999$ and an RMSECV of 0.00272. The low errors associated with the training set models' cross-validation indicate the model's validity for use in measuring the unknown

Table 2. Statistics and Details for PLS Models Created for the Training Set of Averaged Raman Spectra

analyte	RMSEC	RMSECV	R^2 (cal, CV)	latent variables	spectral preprocessing
hydrogen peroxide	0.0218	0.0258	0.9988, 0.9983	3	1st derivative; normalization to water band; mean center
cellobiose	0.00206	0.00272	0.9997, 0.9995	2	1st derivative; normalization to water band; mean center

concentrations in an irradiated sample. The statistics and details for model performance are listed in Table 2.

The PLS models described above were applied to the on-line Raman spectral data of the irradiation. While training sets and initial grab sample analyses indicated excellent potential for model performance, a number of complicating factors were observed during the real-time monitoring of the sample irradiation. Firstly, the probe was set in the vessel such that the window face was horizontal. Bubbles formed as a part of the chemical reaction and bubble collection on the probe window periodically obscured solution interrogation. It is suspected that this bubble formation reduced spectral intensity and altered the ratios of analyte peaks. Furthermore, cosmic spikes were observed likely due to stray radiation from nearby exposure facilities. These spikes occur at random wavenumbers and often occurred directly on or near an analyte peak, creating a high-intensity, false response at wavenumbers of interest.⁷⁹ These spectra are shown in Figure S3.

In order to reduce the impact of cosmic rays, the on-line run spectra were averaged by 20. The dataset was otherwise preprocessed using the same methods as the training set.

To remove spectra that were egregiously affected by the formation of bubbles on the probe window and by the influence of cosmic rays, a process of Q residual filtering was utilized. Q residuals are a form of metadata that can indicate whether or not a spectral signature differs significantly from the spectra captured in the training sets.⁸⁰ The Eigenvector software used here outputs metadata and statistical analyses along with results from applications of chemometric models. The resulting Q residuals observed after applying the hydrogen peroxide and cellobiose models to the Raman data collected on-line during the irradiation can be seen in Figure 8. The

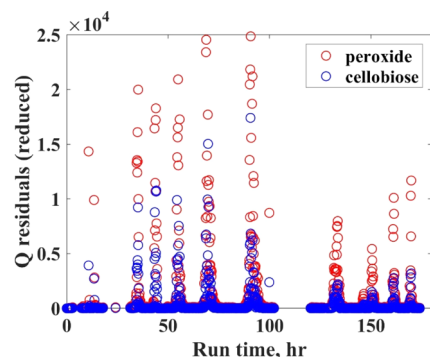


Figure 8. Q -residual values corresponding to the hydrogen peroxide and cellobiose data (displayed in Figure 9), showing the effect of intermittent gas bubble attachment and release at the optical probe tip.

observed patterns in Q residuals align with the theory that bubbles would periodically collect on the windows and obscure Raman measurements, thereby increasing Q residuals. The pattern indicated the growth of bubbles on the probe window and their migration off the window, which happened through two processes: either the bubble grew large enough to migrate off the probe on its own or the researcher paused the

irradiation briefly to tap the probe (dislodging bubbles) during the collection of the grab sample from the first vessel. A cutoff was set to remove results with a reduced Q residual greater than 5×10^{-3} because this data was compromised by the presence of disturbances. The progression from raw spectra to the Q residual filtered spectra can be seen in Figure S3. This process resulted in a matrix of 138 averaged spectra for the peroxide model and 271 averaged spectra for the cellobiose model. These spectra are pulled from throughout the experiment's duration, and they show a marked decrease in cosmic rays directly interfering with the analyte bands, as shown in Figure S3C,F. These factors indicate that much of the variation in the concentrations measured by the model arises from interferences such as bubble formation that occur throughout the experiment and cosmic rays which cause temporally random false readings by the model.

After preprocessing of the spectra and removal of compromised spectra, both peroxide and cellobiose were successfully measured using the chemometric analysis. Figure 9A shows the measured value of hydrogen peroxide by the model across the duration of the irradiation. The negative slope aligns with the trend observed in the grab sample and on-line run spectra, in which the peroxide response peak decreases

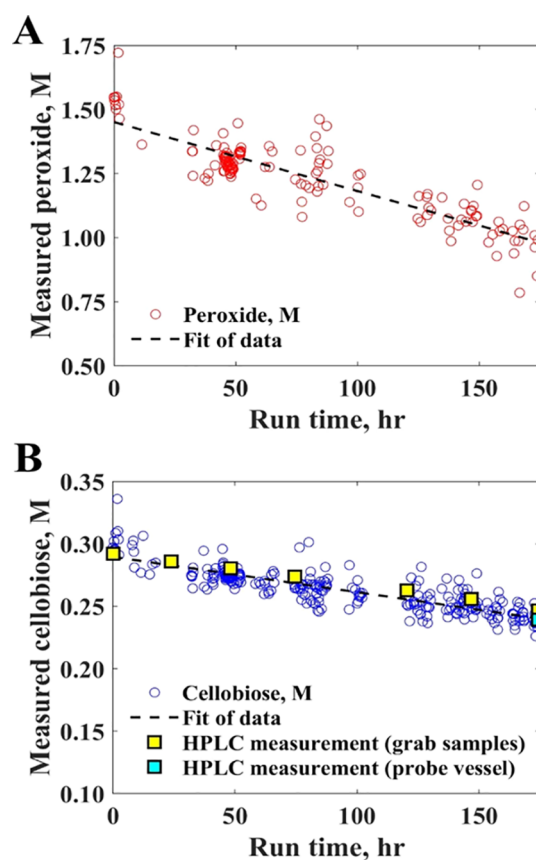


Figure 9. (A) On-line measurement of hydrogen peroxide during γ -irradiation and (B) on-line and grab sample measurements of cellobiose during irradiation experiments.

as the dose increases. Further evidence of model efficacy is seen in Figure 9B, which displays the model's measurement of cellobiose as the irradiation progresses. This plot displays the concentrations of cellobiose in grab samples taken from the grab sample vessel during the ongoing irradiation and measured off-line by HPLC analysis. An offset was applied to the concentrations measured by the HPLC in order to standardize the HPLC measurements to the known starting concentration of the solution in the grab sample vessel before irradiation occurred. The final point on this plot, shown in cyan blue, shows the HPLC measurement of the solution in which the probe was immersed, demonstrating that the two vessels compare favorably despite aliquots of solution being removed from the grab sample vessel throughout the irradiation and the probe vessel remaining undisturbed. The HPLC measurements show good agreement with the line of best fit created by the chemometric model of Raman spectra.

Overall, chemometric PLS models constructed from spectra taken on nonirradiated samples allowed for the measurement of peroxide and cellobiose in situ during the course of the irradiation of cellobiose in hydrogen peroxide. The models' measurements are in good agreement with the quantification performed using HPLC analysis. The chemometric models successfully measured two major components of the system: the oxidant, hydrogen peroxide and the source biomass, cellobiose. Additional models could be constructed for Raman active degradation products, such as levoglucosan or formic acid.⁸¹

3. CONCLUSIONS

Nuclear energy reactors produce unused radiation that can be utilized to drive chemical reactions. The coupling of a chemical plant of radiation-enhanced chemical production alongside a nuclear reactor would create a hybrid reactor with greater economic and environmental benefits than a nuclear reactor alone. Here, chemometric modeling of the Raman spectra collected during the on-line monitoring of the irradiation of cellobiose in hydrogen peroxide provided quantitative information on inorganic and organic compounds in the reaction solution. This work demonstrates the ability of optical spectroscopic on-line monitoring to provide valuable, quantitative, and real-time measurements of the radiation-enhanced degradation. Such monitoring allows for more efficient chemical production, as the chemical system can be optimized in response to the real-time information provided by spectroscopic monitoring. Such on-line monitoring also contributes to creating safer hybrid reactors. The exploration of more complex biomass systems is warranted in order to provide support for the construction of hybrid reactors in the future.

4. EXPERIMENTAL SECTION

4.1. Materials. Cellobiose (>98%), hydrogen peroxide (30% solution), and potential degradation products such as levoglucosan, glucose, and hydroxymethylfurfural (HMF) were purchased from Sigma–Aldrich (St. Louis, MO, USA).

The irradiated samples were composed of solutions of 0.292–0.294 M cellobiose and 1.63 M hydrogen peroxide in 18 MΩ cm DI water.

A set of training solutions, used to build chemometric models, was created. Samples were created to include the original analytes and the expected degradation products that

would be produced during the irradiation. The samples contained hydrogen peroxide, cellobiose, levoglucosan, HMF, and glucose in 18 MΩ cm DI water. This is discussed further below.

4.2. High Exposure Facility. The samples were irradiated in the High Exposure Facility (HEF) at the Pacific Northwest National Laboratory. HEF is a gamma irradiation facility that provides high-dose gamma irradiation with a variety of high-energy gamma sources. The source employed in this work was ⁶⁰Co with a starting activity of 10,000 Ci. The stainless-steel vessels and their position relative to the HEF exposure cone are shown in Figure 2B.

4.3. Equipment. Samples were analyzed using HPLC equipped with a Waters 2414 refractive index detector. A Bio-Rad Aminex HPX-87H ion exclusion column (300 mm × 7.8 mm) was used for analyte separation. Sulfuric acid (0.005 M) was used as the eluent at a flow rate of 0.55 mL/min. The eluent was filtered through a 0.2 μm filter and degassed. The calibration curves for each of the known compounds contained five concentration levels ranging from 0.1 to 2.0 wt %. The R² values were greater than 0.99 for all of the reported analytes. Each calibration was verified with an independently prepared standard run as the control. The recovery of the calibration checks ranged from 93.6 to 108%. Acetic acid, methanol, ethanol, acetone, and methylethylketone were selected as calibration check compounds. The opening/closing continuing calibration verification percent recoveries for these compounds were 94.8 to 102.8%. Curves were plotted using OriginPro 2019b.

Two Raman systems were utilized in this work. Both were acquired from Spectra Solutions Inc. (Norwood, MA, USA), each with a 671 nm excitation laser. Each system contained a transmission VPH grating spectrograph with a thermoelectrically cooled charge-coupled device detector to record the Raman signal from the Raman probe over a spectral range of 200–3800 cm⁻¹. The wavenumber reading for each spectrometer was calibrated using naphthalene, and the resolution of each spectrometer was ~5 cm⁻¹.

4.4. Chemometric Analysis. Spectral preprocessing was conducted using Matlab2019b (Mathworks, Natick, MA, USA), and chemometric models were built using PLS Toolbox 8.7.1 (Eigenvector Research Incorporated, Manson, WA, USA).

■ ASSOCIATED CONTENT

SI Supporting Information

The Supporting Information is available free of charge at <https://pubs.acs.org/doi/10.1021/acsomega.1c04852>.

Single-component HPLC spectra to support compound identification during HPLC of irradiated samples; Raman spectra of grab samples from the reaction of cellobiose and hydrogen peroxide under conditions of no irradiation; and raw spectra acquired on-line during the irradiation of cellobiose and hydrogen peroxide in DI water using a cobalt-60 source (PDF)

■ AUTHOR INFORMATION

Corresponding Author

Heather A. Colburn – Energy and Environment Directorate, Pacific Northwest National Laboratory, Richland, Washington 99352, United States; orcid.org/0000-0003-0399-4728; Email: Heather.colburn@pnnl.gov

Authors

Hope E. Lackey – Energy and Environment Directorate,
Pacific Northwest National Laboratory, Richland,
Washington 99352, United States

Mariefel V. Olarte – Energy and Environment Directorate,
Pacific Northwest National Laboratory, Richland,
Washington 99352, United States; orcid.org/0000-0003-2989-1110

Teresa Lemmon – Energy and Environment Directorate,
Pacific Northwest National Laboratory, Richland,
Washington 99352, United States; orcid.org/0000-0001-6432-4133

Heather M. Felmy – Energy and Environment Directorate,
Pacific Northwest National Laboratory, Richland,
Washington 99352, United States

Samuel A. Bryan – Energy and Environment Directorate,
Pacific Northwest National Laboratory, Richland,
Washington 99352, United States; orcid.org/0000-0002-8826-0880

Amanda M. Lines – Energy and Environment Directorate,
Pacific Northwest National Laboratory, Richland,
Washington 99352, United States

Complete contact information is available at:

<https://pubs.acs.org/10.1021/acsomega.1c04852>

Notes

The authors declare no competing financial interest.

ACKNOWLEDGMENTS

The authors are grateful for the assistance in execution of this work by the staff supporting the PNNL High Exposure Facility, and the support staff that make this type of work possible. This work was supported by PNNL's Energy and Environment Directorate Laboratory Directed Research and Development Funding and was performed at the Pacific Northwest National Laboratory (PNNL) operated by Battelle for the U.S. Department of Energy under Contract DE-AC05-76RL01830.

REFERENCES

- (1) Ruth, M. F.; Zinaman, O. R.; Antkowiak, M.; Boardman, R. D.; Cherry, R. S.; Bazilian, M. D. Nuclear-renewable hybrid energy systems: Opportunities, interconnections, and needs. *Energy Convers. Manage.* **2014**, *78*, 684–694.
- (2) Forsberg, C. Hybrid systems to address seasonal mismatches between electricity production and demand in nuclear renewable electrical grids. *Energy Policy* **2013**, *62*, 333–341.
- (3) Ertör-Akyazı, P.; Adaman, F.; Özkaynak, B.; Zenginobuz, Ü. Citizens' preferences on nuclear and renewable energy sources: Evidence from Turkey. *Energy Policy* **2012**, *47*, 309–320.
- (4) Schmeda-Lopez, D.; McConnaughy, T. B.; McFarland, E. W. Radiation enhanced chemical production: Improving the value proposition of nuclear power. *Energy* **2018**, *162*, 491–504.
- (5) Karakosta, C.; Pappas, C.; Marinakis, V.; Psarras, J. Renewable energy and nuclear power towards sustainable development: Characteristics and prospects. *Renewable Sustainable Energy Rev.* **2013**, *22*, 187–197.
- (6) McConnaughy, T. B.; Shaner, M. R.; McFarland, E. W. A Techno-Economic Analysis of Chemical Processing with Ionizing Radiation. *Chem. Eng. Technol.* **2017**, *40*, 1196–1202.
- (7) Cicia, G.; Cembalo, L.; Del Giudice, T.; Palladino, A. Fossil energy versus nuclear, wind, solar and agricultural biomass: Insights from an Italian national survey. *Energy Policy* **2012**, *42*, 59–66.
- (8) Plant, A. G.; Najdanovic-Visak, V.; Joyce, M. J.; Snoj, L.; Jazbec, A. Producing Useful Chemicals Using a Nuclear Reactor. *EPJ Web Conf.* **2020**, *225*, 09003.
- (9) Dang, V.-D.; Steinberg, M. A Neutron-Gamma Chemonuclear Fusion Reactor. *Nucl. Technol.* **1977**, *36*, 193–199.
- (10) Harmer, D. E.; Beale, J. S.; Pumpelly, C. T.; Wilkinson, B. W. *The Dow Ethyl Bromide Process: An Industrial Application of Radiation Chemistry*; International Atomic Energy Agency, 1963; Vol. 2, pp 205–228.
- (11) Spinks, J. W. T.; Woods, R. J. *An Introduction to Radiation Chemistry*, 3rd ed.; John Wiley and Sons, 1990.
- (12) Steinberg, M. Chemonuclear and Radiation Chemical Process Applications. *Nucl. Appl.* **1969**, *6*, 425–433.
- (13) Betiku, E.; Adetunji, O. A.; Ojumu, T. V.; Solomon, B. O. A comparative study of the hydrolysis of gamma irradiated lignocelluloses. *Braz. J. Chem. Eng.* **2009**, *26*, 251–255.
- (14) Ershov, B. G. Radiation-chemical degradation of cellulose and other polysaccharides. *Russ. Chem. Rev.* **1998**, *67*, 315–334.
- (15) Guo, X.; Li, H.; Yan, H.; Dai, Y.; Luo, X.; Yang, X.; Kong, L. Production of organic carboxylic acids by hydrothermal conversion of electron beam irradiation pretreated wheat straw. *Biomass Convers. Biorefin.* **2020**, *10*, 997–1006.
- (16) Metreveli, A. K.; Metreveli, P. K.; Makarov, I. E.; Ponomarev, A. V. Aromatic products of radiation-thermal degradation of lignin and chitin. *High Energy Chem.* **2013**, *47*, 35–40.
- (17) Ponomarev, A. V.; Kholodkova, E. M.; Metreveli, A. K.; Metreveli, P. K.; Erasov, V. S.; Bludenko, A. V.; Chulkov, V. N. Phase distribution of products of radiation and post-radiation distillation of biopolymers: Cellulose, lignin and chitin. *Radiat. Phys. Chem.* **2011**, *80*, 1186–1194.
- (18) Wang, K.-q.; Xiong, X.-y.; Chen, J.-p.; Chen, L.; Su, X.; Liu, Y. Comparison of gamma irradiation and steam explosion pretreatment for ethanol production from agricultural residues. *Biomass Bioenergy* **2012**, *46*, 301–308.
- (19) Yang, C.; Shen, Z.; Yu, G.; Wang, J. Effect and aftereffect of γ radiation pretreatment on enzymatic hydrolysis of wheat straw. *Bioresour. Technol.* **2008**, *99*, 6240–6245.
- (20) Soomro, A.; Chen, S.; Sun, Z.; Ma, S.; Xiang, W. Chemometric modelling on element compositions and product distributions of cellulose and lignin. *Biomass Convers. Biorefin.* **2021**, *11*, 2233–2246.
- (21) Khan, F.; Ahmad, S. R.; Kronfli, E. Gamma-radiation induced changes in the physical and chemical properties of lignocellulose. *Biomacromolecules* **2006**, *7*, 2303–2309.
- (22) Ponomarev, A. V.; Ershov, B. G. Radiation-induced degradation of cellulose: From partial depolymerization to complete self-disassembly. *Radiat. Phys. Chem.* **2018**, *152*, 63–68.
- (23) Chosdu, R.; Hilmy, N.; Erizal; Erlinda, T. B.; Abbas, B. Radiation and Chemical Pretreatment of Cellulosic Waste. *Radiat. Phys. Chem.* **1993**, *42*, 695–698.
- (24) Hyun Hong, S.; Taek Lee, J.; Lee, S.; Gon Wi, S.; Ju Cho, E.; Singh, S.; Sik Lee, S.; Yeoup Chung, B. Improved enzymatic hydrolysis of wheat straw by combined use of gamma ray and dilute acid for bioethanol production. *Radiat. Phys. Chem.* **2014**, *94*, 231–235.
- (25) Takács, E.; Wojnárovits, L.; Földváry, C.; Hargittai, P.; Borsas, J.; Sajó, I. Effect of combined gamma-irradiation and alkali treatment on cotton-cellulose. *Radiat. Phys. Chem.* **2000**, *57*, 399–403.
- (26) Xin, L. Z.; Kumakura, M. Effect of Radiation Pretreatment on Enzymatic-Hydrolysis of Rice Straw with Low Concentrations of Alkali Solution. *Bioresour. Technol.* **1993**, *43*, 13–17.
- (27) Yin, Y.; Wang, J. Enhancement of enzymatic hydrolysis of wheat straw by gamma irradiation-alkaline pretreatment. *Radiat. Phys. Chem.* **2016**, *123*, 63–67.
- (28) Driscoll, M. S.; Stipanovic, A. J.; Cheng, K.; Barber, V. A.; Manning, M.; Smith, J. L.; Sundar, S. Ionizing Radiation and a Wood-Based Biorefinery. *Radiat. Phys. Chem.* **2014**, *94*, 217–220.
- (29) Chung, B. Y.; Lee, J. T.; Bai, H.-W.; Kim, U.-J.; Bae, H.-J.; Gon Wi, S.; Cho, J.-Y. Enhanced Enzymatic Hydrolysis of Poplar Bark by Combined Use of Gamma Ray and Dilute Acid for Bioethanol Production. *Radiat. Phys. Chem.* **2012**, *81*, 1003–1007.

- (30) Teong, S. P.; Li, X.; Zhang, Y. Hydrogen peroxide as an oxidant in biomass-to-chemical processes of industrial interest. *Green Chem.* **2019**, *21*, 5753–5780.
- (31) Deng, W.; Lobo, R.; Setthapun, W.; Christensen, S. T.; Elam, J. W.; Marshall, C. L. Oxidative Hydrolysis of Cellobiose to Glucose. *Catal. Lett.* **2011**, *141*, 498–506.
- (32) Kane, R. W.; Timpa, J. D. A High-Performance Liquid Chromatography Study of D-Cellobiose Degradation Under Fenton Conditions. *J. Carbohydr. Chem.* **1992**, *11*, 779–797.
- (33) Dutra, E. D.; Santos, F. A.; Alencar, B. R. A.; Reis, A. L. S.; de Souza, R. d. F. R.; Aquino, K. A. d. S.; Morais, M. A., Jr.; Menezes, R. S. C. Alkaline hydrogen peroxide pretreatment of lignocellulosic biomass: status and perspectives. *Biomass Convers. Biorefin.* **2018**, *8*, 225–234.
- (34) Chen, C.-T.; Nguyen, C. V.; Wang, Z.-Y.; Bando, Y.; Yamauchi, Y.; Bazziz, M. T. S.; Fatehmulla, A.; Farooq, W. A.; Yoshikawa, T.; Masuda, T.; Wu, K. C.-W. Hydrogen Peroxide Assisted Selective Oxidation of 5-Hydroxymethylfurfural in Water under Mild Conditions. *ChemCatChem* **2018**, *10*, 361–365.
- (35) Lucas, M.; Hanson, S. K.; Wagner, G. L.; Kimball, D. B.; Rector, K. D. Evidence for room temperature delignification of wood using hydrogen peroxide and manganese acetate as a catalyst. *Bioresour. Technol.* **2012**, *119*, 174–180.
- (36) Dutta, S.; Wu, L.; Mascial, M. Efficient, metal-free production of succinic acid by oxidation of biomass-derived levulinic acid with hydrogen peroxide. *Green Chem.* **2015**, *17*, 2335–2338.
- (37) Verardi, A.; Blasi, A.; Marino, T.; Molino, A.; Calabrò, V. Effect of steam-pretreatment combined with hydrogen peroxide on lignocellulosic agricultural wastes for bioethanol production: Analysis of derived sugars and other by-products. *J. Energy Chem.* **2018**, *27*, 535–543.
- (38) Sjostrom, E. *Wood Chemistry: Fundamentals and Applications*; Gulf Professional Publishing, 1993.
- (39) Von Sonntag, C.; Dizdaroglu, M.; Schulte-Frohlinde, D. Radiation-Chemistry of Carbohydrates VIII Gamma-Radiolysis of Cellobiose in N₂O-Saturated Aqueous-Solution. II Quantitative Measurements - Mechanisms of Radical-Induced Scission of Glycosidic Linkage. *Z. Naturforsch. B* **1976**, *31*, 857–864.
- (40) Kowal, K.; Potemski, S.; Stano, P. M. *A General Framework for Integrated Risk Assessment of Nuclear/Non-nuclear Combined Installations on Market-Oriented Nuclear Industry*; CRC Press, 2018; pp 1623–1628.
- (41) Wang, Q.; Li, R.; He, G. Research status of nuclear power: A review. *Renewable Sustainable Energy Rev.* **2018**, *90*, 90–96.
- (42) Corrado, J. K. The Intersection of Advancing Technology and Human Performance. *J. Nucl. Eng. Radiat. Sci.* **2020**, *7*, 010801.
- (43) Casella, A. J.; Ahlers, L. R. H.; Campbell, E. L.; Levitskaia, T. G.; Peterson, J. M.; Smith, F. N.; Bryan, S. A. Development of Online Spectroscopic pH Monitoring for Nuclear Fuel Reprocessing Plants: Weak Acid Schemes. *Anal. Chem.* **2015**, *87*, 5139–5147.
- (44) Lines, A. M.; Adams, S. R.; Casella, A. J.; Sinkov, S. I.; Lumetta, G. J.; Bryan, S. A. Electrochemistry and Spectroelectrochemistry of the Pu (III/IV) and (IV/VI) Couples in Nitric Acid Systems. *Electroanalysis* **2017**, *29*, 2744–2751.
- (45) Lines, A. M.; Hall, G. B.; Asmussen, S.; Allred, J.; Sinkov, S.; Heller, F.; Gallagher, N.; Lumetta, G. J.; Bryan, S. A. Sensor Fusion: Comprehensive Real-Time, On-Line Monitoring for Process Control via Visible, Near-Infrared, and Raman Spectroscopy. *ACS Sens.* **2020**, *5*, 2467–2475.
- (46) Lackey, H. E.; Nelson, G. L.; Lines, A. M.; Bryan, S. A. Reimagining pH Measurement: Utilizing Raman Spectroscopy for Enhanced Accuracy in Phosphoric Acid Systems. *Anal. Chem.* **2020**, *92*, 5882–5889.
- (47) Chang, H.; Wohlschlager, L.; Csarman, F.; Ruff, A.; Schuhmann, W.; Scheiblbrandner, S.; Ludwig, R. Real-Time Measurement of Cellobiose and Glucose Formation during Enzymatic Biomass Hydrolysis. *Anal. Chem.* **2021**, *93*, 7732–7738.
- (48) Cruys-Bagger, N.; Ren, G.; Tatsumi, H.; Baumann, M. J.; Spodsborg, N.; Andersen, H. D.; Gorton, L.; Borch, K.; Westh, P. An amperometric enzyme biosensor for real-time measurements of cellobiohydrolase activity on insoluble cellulose. *Biotechnol. Bioeng.* **2012**, *109*, 3199–3204.
- (49) Olsen, S. N.; Lumby, E.; McFarland, K.; Borch, K.; Westh, P. Kinetics of Enzymatic High-Solid Hydrolysis of Lignocellulosic Biomass Studied by Calorimetry. *Appl. Biochem. Biotechnol.* **2011**, *163*, 626–635.
- (50) Jimenez-Flores, R.; Fake, G.; Carroll, J.; Hood, E.; Howard, J. A novel method for evaluating the release of fermentable sugars from cellulosic biomass. *Enzyme Microb. Technol.* **2010**, *47*, 206–211.
- (51) Zhang, X.; Ma, J.; Ji, Z.; Yang, G.-H.; Zhou, X.; Xu, F. Using confocal Raman microscopy to real-time monitor poplar cell wall swelling and dissolution during ionic liquid pretreatment. *Microsc. Res. Tech.* **2014**, *77*, 609–618.
- (52) Saar, B. G.; Zeng, Y.; Freudiger, C. W.; Liu, Y.-S.; Himmel, M. E.; Xie, X. S.; Ding, S.-Y. Label-Free, Real-Time Monitoring of Biomass Processing with Stimulated Raman Scattering Microscopy. *Angew. Chem., Int. Ed.* **2010**, *49*, 5476–5479.
- (53) Lähdetie, A. Wood biomass characterization by Raman spectroscopy. Ph.D. Thesis, Aalto University, 2013.
- (54) Wójciak, A.; Kasprzyk, H.; Sikorska, E.; Krawczyk, A.; Sikorski, M.; Weselucha-Birczyńska, A. FT-Raman, FT-infrared and NIR spectroscopic characterization of oxygen-delignified kraft pulp treated with hydrogen peroxide under acidic and alkaline conditions. *Vib. Spectrosc.* **2014**, *71*, 62–69.
- (55) Lupoi, J. S.; Gjersing, E.; Davis, M. F. Evaluating Lignocellulosic Biomass, Its Derivatives, and Downstream Products with Raman Spectroscopy. *Front. Bioeng. Biotechnol.* **2015**, *3*, 50.
- (56) Bryant, D. N.; Morris, S. M.; Leemans, D.; Fish, S. A.; Taylor, S.; Carvell, J.; Todd, R. W.; Logan, D.; Lee, M.; Garcia, N.; Ellis, A.; Gallagher, J. A. Modelling real-time simultaneous saccharification and fermentation of lignocellulosic biomass and organic acid accumulation using dielectric spectroscopy. *Bioresour. Technol.* **2011**, *102*, 9675–9682.
- (57) Lines, A. M.; Tse, P.; Felmy, H. M.; Wilson, J. M.; Shafer, J.; Denslow, K. M.; Still, A. N.; King, C.; Bryan, S. A. Online, Real-Time Analysis of Highly Complex Processing Streams: Quantification of Analytes in Hanford Tank Sample. *Ind. Eng. Chem. Res.* **2019**, *58*, 21194–21200.
- (58) Bryan, S. A.; Levitskaia, T. G.; Casella, A. J.; Peterson, J. M.; Johnsen, A. M.; Lines, A. M.; Thomas, E. M. Spectroscopic on-line monitoring for process control and safeguarding of radiochemical streams in nuclear fuel reprocessing facilities. In *Advanced Separation Techniques for Nuclear Fuel Reprocessing and Radioactive Waste Treatment*; Nash, K. L., Lumetta, G. J., Eds.; Woodhead Publishing, 2011; pp 95–119.
- (59) Bryan, S. A.; Levitskaia, T. G.; Schwantes, J. M.; Orton, C. R.; Peterson, J. M.; Casella, A. J. Monitoring, Controlling and Safeguarding Radiochemical Streams at Spent Fuel Reprocessing Facilities, Part 1: Optical Spectroscopic Methods, last revised February 2012. <https://www.osti.gov/biblio/1054426> (accessed Feb 12, 2020).
- (60) Parruzot, B.; Ryan, J. V.; Lines, A. M.; Bryan, S. A.; Neeway, J. J.; Chatterjee, S.; Lukins, C. D.; Casella, A. J. Method for the in situ Measurement of pH and Alteration Extent for Aluminoborosilicate Glasses Using Raman Spectroscopy. *Anal. Chem.* **2018**, *90*, 11812–11819.
- (61) Agarwal, U.; Weinstock, I.; Atalla, R. H. FT-Raman Spectroscopy: A Rapid Non-invasive Technique for Direct Measurement of Lignin in Kraft Pulp. *International Pulp Bleaching Conference*, 1996; Vol. 2(22), pp 531–535.
- (62) Agarwal, U. P. Raman imaging to investigate ultrastructure and composition of plant cell walls: distribution of lignin and cellulose in black spruce wood (*Picea mariana*). *Planta* **2006**, *224*, 1141.
- (63) Ona, T.; Sonoda, T.; Ito, K.; Shibata, M.; Kato, T.; Ootake, Y.; Tamai, Y.; Kojima, Y. Rapid prediction of native wood pulp properties by Fourier transform Raman spectroscopy. *J. Pulp Pap. Sci.* **2000**, *26*, 43–47.

- (64) Zhang, X.; Chen, S.; Xu, F. Combining Raman Imaging and Multivariate Analysis to Visualize Lignin, Cellulose, and Hemicellulose in the Plant Cell Wall. *J. Visualized Exp.* **2017**, *124*, 55910.
- (65) Agarwal, U. P. Analysis of Cellulose and Lignocellulose Materials by Raman Spectroscopy: A Review of the Current Status. *Molecules* **2019**, *24*, 1659.
- (66) Tse, P.; Bryan, S. A.; Bessen, N. P.; Lines, A. M.; Shafer, J. C. Review of on-line and near real-time spectroscopic monitoring of processes relevant to nuclear material management. *Anal. Chim. Acta* **2020**, *1107*, 1–13.
- (67) Bondy, A. L.; Craig, R. L.; Zhang, Z.; Gold, A.; Surratt, J. D.; Ault, A. P. Isoprene-Derived Organosulfates: Vibrational Mode Analysis by Raman Spectroscopy, Acidity-Dependent Spectral Modes, and Observation in Individual Atmospheric Particles. *J. Phys. Chem. A* **2018**, *122*, 303–315.
- (68) Workman, J. J. Infrared and Raman spectroscopy in paper and pulp analysis. *Appl. Spectrosc. Rev.* **2001**, *36*, 139–168.
- (69) Venkateswaran, S. Raman Spectrum of Hydrogen Peroxide. *Nature* **1931**, *127*, 406.
- (70) Taylor, R. C.; Cross, P. C. Raman Spectra of Hydrogen Peroxide in Condensed Phases. I. The Spectra of the Pure Liquid and Its Aqueous Solutions. *J. Chem. Phys.* **1956**, *24*, 41–44.
- (71) Xie, H.-b.; Pincu, M.; Brauer, B.; Gerber, R. B.; Bar, I. Raman and infrared spectra of cellobiose in the solid state: What can be learned from single-molecule calculations? *Chem. Phys. Lett.* **2011**, *514*, 284–290.
- (72) Lines, A. M.; Nelson, G. L.; Casella, A. J.; Bello, J. M.; Clark, S. B.; Bryan, S. A. Multivariate Analysis To Quantify Species in the Presence of Direct Interferents: Micro-Raman Analysis of HNO₃ in Microfluidic Devices. *Anal. Chem.* **2018**, *90*, 2548–2554.
- (73) Lumetta, G. J.; Allred, J. R.; Bryan, S. A.; Hall, G. B.; Levitskaia, T. G.; Lines, A. M.; Sinkov, S. I. Simulant testing of a co-decontamination (CoDCon) flowsheet for a product with a controlled uranium-to-plutonium ratio. *Sep. Sci. Technol.* **2019**, *54*, 1977–1984.
- (74) Nelson, G. L.; Lines, A. M.; Bello, J. M.; Bryan, S. A. Online Monitoring of Solutions Within Microfluidic Chips: Simultaneous Raman and UV-Vis Absorption Spectroscopies. *ACS Sens.* **2019**, *4*, 2288–2295.
- (75) Uddin, M. N.; Nayeem, J.; Islam, M. S.; Jahan, M. S. Rapid determination method of dissolving pulp properties by spectroscopic data and chemometrics. *Biomass Convers. Biorefin.* **2019**, *9*, 585–592.
- (76) Takayama, M.; Johjima, T.; Yamanaka, T.; Wariishi, H.; Tanaka, H. Fourier transform Raman assignment of guaiacyl and syringyl marker bands for lignin determination. *Spectrochim. Acta, Part A* **1997**, *53*, 1621–1628.
- (77) Edimecheva, I. P.; Kisel, R. M.; Shadyro, O. I.; Kazem, K.; Murase, H.; Kagiya, T. Homolytic cleavage of the O-glycoside bond in carbohydrates: A steady-state radiolysis study. *J. Radiat. Res.* **2005**, *46*, 319–324.
- (78) Savitzky, A.; Golay, M. J. E. Smoothing + Differentiation of Data by Simplified Least Squares Procedures. *Anal. Chem.* **1964**, *36*, 1627–1639.
- (79) Phillips, G. R.; Harris, J. M. Polynomial filters for data sets with outlying or missing observations: application to charge-coupled-device-detected Raman spectra contaminated by cosmic rays. *Anal. Chem.* **1990**, *62*, 2351–2357.
- (80) Wise, B. M.; Gallagher, N. B. The process chemometrics approach to process monitoring and fault detection. *J. Process Control* **1996**, *6*, 329–348.
- (81) Bartholomew, R. J. Raman spectral studies of solutions of formic acid and methyl formate. Ph.D.Thesis, University of Waterloo, Waterloo, Ontario, Canada, 1996.